Dalton Transactions

ROYAL SOCIETY OF CHEMISTRY

PERSPECTIVE

View Article Online
View Journal | View Issue

Cite this: *Dalton Trans.*, 2020, **49**, 2381

Recent advances in metalloporphyrin-based catalyst design towards carbon dioxide reduction: from bio-inspired second coordination sphere modifications to hierarchical architectures

Philipp Gotico, [a] Zakaria Halime *[b] and Ally Aukauloo *[a,b]

Received 11th December 2019,
Accepted 22nd January 2020

DOI: 10.1039/c9dt04709c

rsc.li/dalton

Research in the development of new molecular catalysts for the selective transformation of CO_2 to reduced forms of carbon is attracting enormous interest from chemists. Molecular catalyst design hinges on the elaboration of ligand scaffolds to manipulate the electronic and structural properties for the fine tuning of the reactivity pattern. A cornucopia of ligand sets have been designed along this line and more and more are being reported. In this quest, the porphyrin molecular platform has been under intensive focus due to the unmatched catalytic properties of metalloporphyrins. There have been rapid advances in this particular field during the last few years wherein both electronic and structural aspects in the second coordination spheres have been addressed to shift the overpotential and improve the catalytic rates and product selectivity. Metalloporphyrins have also attracted much attention in terms of the elaboration of hybrid materials for heterogeneous catalysis. Here too, some promising activities have made metalloporphyrin derivatives serious candidates for technological implementation. This review collects the recent advances centred around the chemistry of metalloporphyrins for the reduction of CO_2.

[a]*Institut de Biologie Intégrative de la Cellule (I2BC), Institut des Sciences du Vivant Frédéric-Joliot, CEA Saclay, Gif-sur-Yvette 91191, France.*
E-mail: ally.aukauloo@u-psud.fr
[b]*Institut de Chimie Moléculaire et des Matériaux d'Orsay (UMR CNRS 8182), Université Paris-Sud, Orsay 91405, France*

1. Introduction

Intense global efforts are being put in place to address climate change which is already affecting the environment in a big way

Philipp Gotico

Philipp Gotico is a double-degree holder of BS in Chemistry and Materials Science & Engineering from the Ateneo de Manila University in the Philippines. He is a multiple-diploma holder as a SERP-Chem Erasmus Mundus MS student getting specializations from the University of Genova (Italy), University of Porto (Portugal), and University of Paris-Saclay (France). He recently finished his PhD in Chemistry from the French Alternative Energies and Atomic Energy Commission (CEA Saclay) with an IRTELIS fellowship. He is interested in the field of environmental sustainability, from topics on solid waste and wastewater management, and now on bio-inspired strategies to address the energy crisis and global warming.

Zakaria Halime

Zakaria Halime received his BS in Chemistry from the University of Fes in Morocco, and his PhD in Chemistry from the University of Rennes 1 in France. After his graduation, he joined the group of Kenneth Karlin at Johns Hopkins University in Baltimore, USA, and then the group of Shunichi Fukuzumi at the Osaka University in Japan as a Post-doc Researcher. In 2016, he was appointed as a CNRS Senior Researcher joining the Artificial Photosynthesis group at the ICMMO Institute, University of Paris-Saclay. He is currently interested in photo- and electro-catalytic reduction of small molecules toward sustainable fuels.

and will persist to worsen life on this earth.[1] Carbon dioxide (CO_2) capture, conversion, storage, and utilization technologies have been proposed with an emphasis on the role of the latter in driving a global scale implementation of low-carbon and energy-efficient chemical and fuel production.[2,3] In light of this call, artificial photosynthesis is an ideal resource-efficient solution, trying to mimic how plants use sustainable sources of sunlight, CO_2 and water to drive the production of energy-rich carbohydrates. As such, promising research efforts have been intensified in reducing CO_2 to similar energy-rich fuels and chemical feedstocks through electro- and photo-catalytic routes. This strategy has resulted in a closed carbon-recycling loop, which is able to transform waste CO_2 emissions into useful products. Integrating this approach with a renewable solar energy source then results in an ideal net negative carbon footprint, and simultaneously addresses the critical concern on the intermittency of the solar energy supply.

The first basic question we need to raise is how do we transform CO_2? A look into the molecular orbital diagram of CO_2 shows fully filled bonding and nonbonding σ and π orbitals, rendering a highly stable molecule (Fig. 1a). The initial step to activate and transform the molecule involves an electron transfer (*i.e.* a reduction process) that occupies the anti-bonding σ* lowest unoccupied molecular orbital (LUMO). This causes an increase in the C–O distance, manifested in the bending of the initially linear molecule.[4] This bent molecule can then more easily interact with electrophiles and nucleophiles through its charge-localized frontier orbitals.

This one-electron reduction of CO_2 to $CO_2^{\bullet-}$, however, is a highly endergonic reaction occurring at a reduction potential of $E^\circ = -1.90$ V *vs.* NHE (Fig. 1b). This is due to a large reorganizational barrier between the linear molecule and bent radical anion. However, performing multi-proton and multi-electron steps is more favourable than single electron reduction because they can lead to thermodynamically more stable molecules like carbon monoxide (CO), formic acid (HCOOH), formaldehyde (HCOH), methanol (CH_3OH), and methane (CH_4) as products. This thermodynamic ease, however, comes with a kinetic cost of bringing together all the protons and electrons in appropriate pathways to result in the desired reaction. As such, to transform CO_2 by overcoming the thermodynamic and kinetic barriers of its reduction, catalysts are needed to stabilize intermediate transition states.

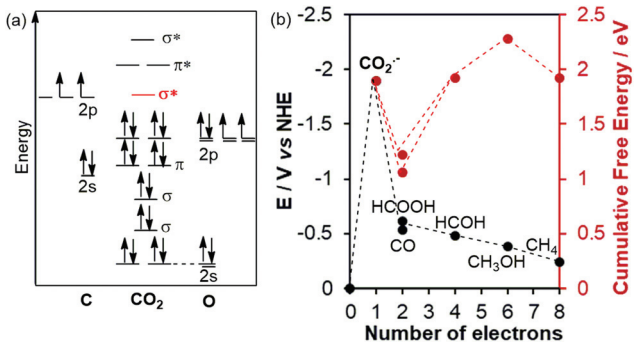

Fig. 1 (a) Molecular orbital diagram of a carbon dioxide molecule and (b) the thermodynamic requirements for its activation and succeeding reduction processes.

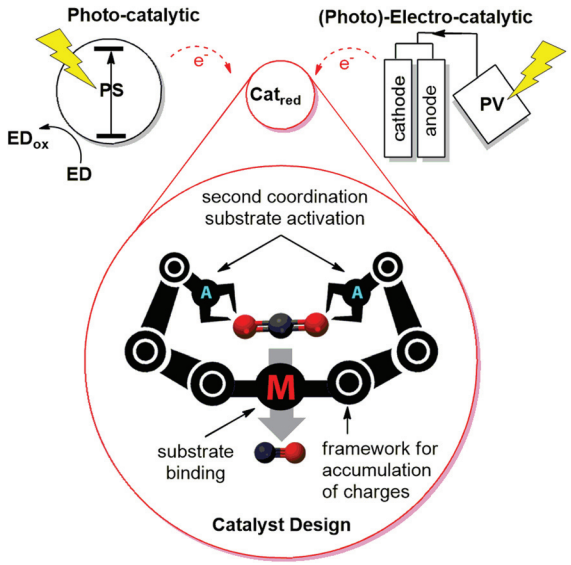

Fig. 2 Simplified diagrams for the photo- and (photo)-electro-catalytic approaches in reducing CO_2 with an overarching theme of catalyst design. (ED = electron donor, PS = photosensitizer, Cat_{red} = reduction catalyst, Cat_{ox} = oxidation catalyst and PV = photovoltaics).

Ally Aukauloo

Ally Aukauloo is a professor in Coordination and Bioinorganic Chemistry at the University of Paris-Saclay and a Scientific Counsellor at the French Alternative Energies and Atomic Energy Commission (CEA Saclay). Responsible for the Artificial Photosynthesis Group, he and his colleagues are developing molecular chemistry to capture and convert sunlight into a chemical potential to perform multi-electronic catalysis for the oxidation of water, production of H_2 and reduction of CO_2 to a fuel.

In addition, energy is still needed to be introduced into the reaction mixture to drive the reduction reactions because of the intrinsic overpotential of catalytic systems. The overpotential corresponds to the energetic barrier to overcome before any redox electrochemical reaction can take place. The energy is ideally supplied by a renewable solar energy resource, standing as one of the pillars of artificial photosynthesis. Two approaches are envisioned, as shown in Fig. 2. One is a photocatalytic approach which involves a photosensitizer (PS) capable of absorbing light and creating charge separated

states (electrons and holes). The holes are replenished by an electron donor (ED), and the electrons are used to activate a reduction catalyst (Cat_{red}) for CO_2 reduction. On the other hand, an electro-catalytic system takes leverage of advances in photovoltaics, which is able to convert light energy to electricity and deliver the necessary electrons to the Cat_{red} in an electrolyser-type configuration.

Central to these approaches is the design of catalysts that can efficiently and selectively reduce CO_2. Most of the CO_2 reduction catalysts contain a central transition metal atom that is supported by a coordinated ligand framework. The metal centre usually acts as the point of binding for the CO_2 substrate and it is typically responsible for transferring the electrons to the substrate. Equally important is the ligand framework which supports and stabilizes the reduced metal and/or can also be the locus for the accumulation of charges in its framework henceforth allowing the storage of multiple reducing equivalents across the molecule. They are generally categorized into two grand families: innocent and non-innocent ligands. Aza-macrocycles such as cyclam, phosphines, and sulphur-containing ligands constitute the former ligand sets while π-containing systems such as porphyrins and similar macrocyclic ligands (phthalocyanines or azaporphyrazines), and polypyridyl ligands (*e.g.* bipyridines, phenanthrolines, terpyridines, quaterpyridines, *etc.*) constitute the latter. Recently, vast literature studies[5–13] have been reviewing the different combinations of transition metals and ligand frameworks employed to reduce carbon dioxide.

This review article will present recent advances in the catalyst design of metalloporphyrin-based CO_2 reduction catalysts for several reasons: (i) they are biologically known to store multiple charges[14] that would be beneficial for addressing the multi-electron steps involved in CO_2 reduction processes, (ii) they have been extensively studied because of the ease and variety of peripheral ligand modifications without significantly modifying the first coordination sphere functionalities, and (iii) they are more fairly compared within their families because of well-established benchmarking schemes.[15–18] Current strategies in homogenous catalysis using bio-inspired second coordination sphere modifications and further developments towards hierarchical architectures in heterogeneous catalysis will be comprehensively examined to provide general guidelines and future opportunities for improving the efficiency and selectivity of CO_2 reduction catalysts.

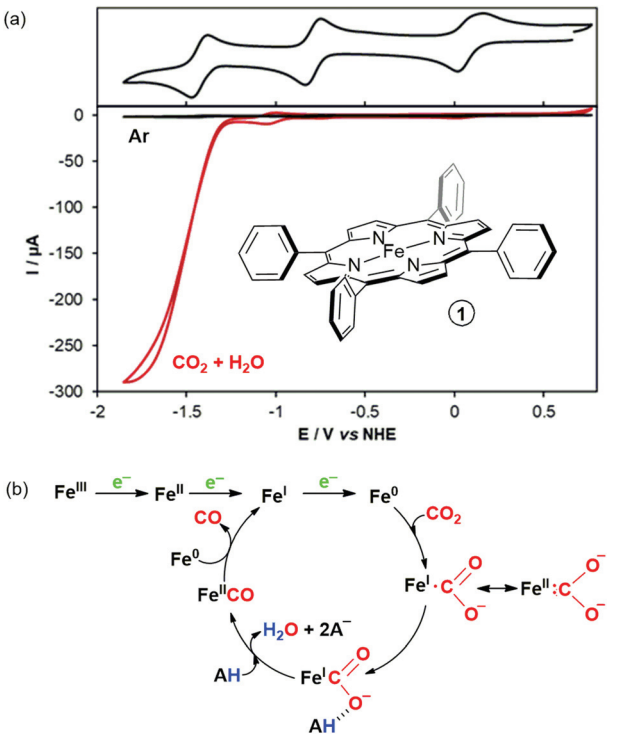

Fig. 3 (a) Cyclic voltammetry of iron tetraphenylporphyrin (FeTPP, **1**) in dimethylformamide containing 0.1 M $TBAPF_6$ under argon (black) and upon CO_2-saturation and addition of 5.5 M H_2O (red), with (b) the proposed mechanism.

2. Homogenous CO_2 reduction

2.1. Mechanism of CO_2-to-CO electrocatalytic reduction by iron-tetraphenylporphyrins

Investigations on the use of metalloporphyrins for the reduction of CO_2 date back to the early 80s[19] and it was the pioneering electrochemical and mechanistic studies by Savéant and coll. on iron(III) tetraphenylporphyrin (FeTPP, catalyst **1**) that boosted further developments.[20] The efficient, selective, and well-characterized electrochemical response of this molecular catalyst, and a variety of opportunities for ligand modifications and catalytic improvements paved the way for the seminal use of such platforms for research studies in the field of CO_2 reduction catalysis.

In a general proposed mechanism, **1** undergoes three reversible reductions as evidenced by three reversible peaks in its cyclic voltammogram (Fig. 3a). These peaks correspond to the formal reductions from Fe^{III} to Fe^{II} to Fe^{I} and finally to the Fe^0 active form. Recent reports from the group of Neese using a comprehensive set of spectroscopic techniques and by computational studies suggest that the last two electrons reside in the π* orbitals of the porphyrin ligand.[21,22] As such, the last two redox couples can be formulated as $[Fe^{II}TPP]/[Fe^{II}(TPP^{\bullet})]^-$ and $[Fe^{II}(TPP^{\bullet})]^-/[Fe^{II}(TPP^{\bullet\bullet})]^{2-}$. Since these electrons are delocalized in the conjugated macrocycle, the corresponding electron transfer will involve marginal geometric distortions of the ligand, and hence a lower reorganizational energy.

The formal Fe^0 species reacts with the CO_2 substrate producing two mesomeric forms: $[Fe^{I}(CO_2^{\bullet})]^{2-}$ and $[Fe^{II}(CO_2^{\bullet\bullet})]^{2-}$ as shown in Fig. 3b. Though there has been no reported experimental evidence of the CO_2 adduct for **1**, yet,[23–25] it was proposed that the reaction goes through the Fe^{I} dissymmetrical adduct, stabilized by a hydrogen bond donor, rather than the Fe^{II} symmetrical adduct.[26] It is then followed by a concerted process of protonation and intramolecular electron transfer, breaking one of the C–O bonds to form a Fe^{II}–CO intermedi-

ate, as proposed by the group of Savéant based on cyclic voltammetry and isotopic H/D studies. This underlines the importance of Lewis acids (*e.g.* Mg^{2+})[27] and Brønsted acids (*e.g.* H_2O, PhOH, and $CF_3CH_2CO_2H$)[28,29] in improving the efficiency and lifetime of the catalyst as initially reported. CO is released after homogeneous one-electron reduction by another Fe^0 species in a comproportionation process, closing the catalytic cycle.[18]

The group of Dey have successfully characterized two intermediates involved in the proposed catalytic cycle using a modified iron porphyrin bearing distal hydrogen bonding pockets (catalyst **24**, Fig. 8).[25] Resonance Raman spectra (recorded at −95 °C) and DFT calculations suggested an initial symmetrical Fe^{II}–CO_2^{2-} intermediate, a resonance form of the initially proposed dissymmetrical intermediate. This intermediate is similarly subjected to a protonation step to form the Fe^{II}–COOH intermediate. The trapped intermediates are specific to the conditions employed in the study (solvent, proton source and temperature) but they are generally in line with the proposed mechanism for iron porphyrins.

2.2. Benchmarking of catalyst performance

The group of Savéant have also developed a benchmarking strategy to easily and fairly compare the electrocatalytic CO_2 reduction performance using foot-of-the-wave (FOW) analysis of the cyclic voltammogram of the catalytic system.[15,17,26,30] This quick evaluation technique gives an indication as to how fast a catalytic system can be driven in terms of the catalytic rate constant (k_{cat}) and turnover frequency (TOF) preventing any contributions from side phenomena such as substrate consumption, catalyst deactivation, and/or product inhibition. The FOW analysis has been successfully applied to a variety of modified iron-porphyrin catalysts with estimations close to those obtained from bulk electrolysis experiments.[31,32]

The analysis is based on the linear correlation between i/i_p^0 and $1/\{1 + \exp[F/RT(E - E_{cat}^0)]\}$ where i is the catalytic current in the presence of CO_2, i_p^0 is the peak current in the absence of CO_2, F is the Faraday constant, R is the gas constant, T is the absolute temperature, E is the applied potential, and E_{cat}^0 is the standard potential of the reversible reduction peak of the active form of the catalyst (*i.e.* $Fe^{I/0}$ couple).

$$\frac{i}{i_p^0} = \frac{2.24\sqrt{\frac{RT}{F\nu}k_{cat}C_{cat}^0}}{1 + \exp\left[\frac{F}{RT}\left(E - E_{cat}^0\right)\right]}$$

Plotting i/i_p^0 *vs.* $1/\{1 + \exp[F/RT(E - E_{cat}^0)]\}$ gives rise to a straight line with a slope = $2.24(RT/F\nu)^{0.5}(k_{cat}C_{cat}^0)^{0.5}$ where ν is the scan rate in V s^{-1} and C_{cat}^0 is the initial concentration of the substrate (*i.e.* CO_2). From this slope, k_{cat} can be determined, and consequently a catalytic Tafel plot can be traced by plotting log TOF *vs.* overpotential, η (*i.e.* $\eta = E_{CO_2/CO}^0 - E$, where $E_{CO_2/CO}^0$ is the thermodynamic potential for the CO_2 reduction process involved and E is the applied potential):

$$TOF_{max} = k_{cat}C_{cat}^0$$

$$TOF = \frac{TOF_{max}}{1 + \exp\left[\frac{F}{RT}\left(E_{cat}^0 - E_{CO_2/CO}^0 - \eta\right)\right]}$$

at

$$\eta = 0, \log TOF_0 = \left[\log TOF_{max} - \frac{F}{RT\ln 10}\left(E_{CO_2/CO}^0 - E_{cat}^0\right)\right]$$

$$\log TOF = \left(\frac{F}{RT\ln 10}\right)\eta + \log TOF_0$$

The plot of log TOF *vs.* η (Fig. 4a) shows two asymptotes: at large overpotentials, log TOF → log TOF_{max}, and at low overpotentials, log TOF → log TOF_0 + $\eta(F/RT\ln 10)$, where TOF_0 is an intrinsic descriptor of the catalyst operating at zero overpotential. As such, by just knowing E_{cat}^0 and TOF_0 or TOF_{max} of the system, one can retrace a catalytic Tafel plot and evaluate the catalytic performance of the catalyst. With the goal of improving the catalytic rate (higher TOF_0 or TOF_{max}) and lowering the overpotential of the system, a good catalyst would be envisioned to have a catalytic Tafel plot shifted upwards to the left, as shown in Fig. 4b.

For example, a classical strategy of lowering the overpotential of a catalyst is through the modification of the porphyrin ligand by incorporating substituents that can induce through-structure electronic effects. For example, the introduction of electron withdrawing groups such as fluorine atoms is expected to lower the overpotential because this lowers the electron density near the metal active site. Thus, it is easier to inject an electron into the catalyst, shifting the reduction potential anodically which results in a lower overpotential. This can be observed for the addition of an increasing number of fluorine atoms from 5 to 20 (catalysts **2**, **3**, **4**, and **5**), resulting in a lower overpotential compared to that of the nonfunctionalized catalyst **1** (the leftward shift of the catalytic Tafel plot in Fig. 5a).[33–36] This occurs, however, with a decrease in the catalytic activity (the downward shift of the Tafel plot) due to the decrease in the nucleophilicity of the active form of the catalyst and its ability to activate the CO_2 substrate.

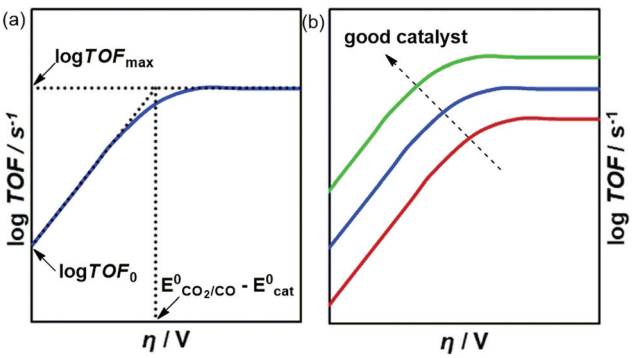

Fig. 4 (a) Catalytic Tafel plot established based on the catalytic parameters estimated by foot-of-the-wave (FOW) analysis with (b) the features of a good catalyst.

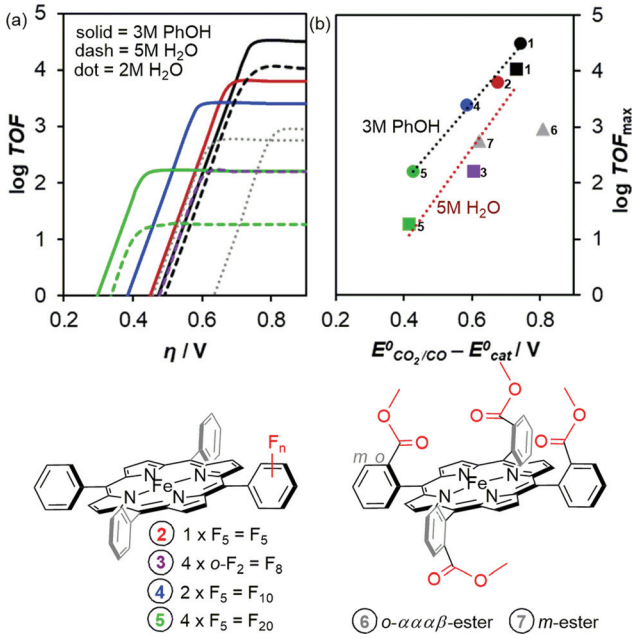

Fig. 5 (a) Catalytic Tafel plots of iron porphyrins modified with fluorine or ester groups with their structures shown at the bottom. (b) Correlation of TOF_{max} with the catalytic potential E^0_{cat} showing through-structure substituent effects. Conditions: DMF with 3 M PhOH (circle) or 5 M H_2O (square) or 2 M H_2O (triangle). Colour legends between (a) and (b) are related to the indicated structures.

An easier comparison of the overlapping catalytic Tafel plots of Fig. 5a can be made by plotting the log TOF_{max} of the catalyst and the overpotential related to the catalytic redox couple ($\eta' = E^0_{CO_2/CO} - E^0_{cat}$), as shown in Fig. 5b. This data point is simply the point of intersection between the two asymptotes of the catalytic Tafel plot. Even though this data point lies beyond the Tafel plot, the ease of identification of such a correlation point, which still includes the characteristic catalytic information, will become useful especially when comparing numerous catalysts. As shown in Fig. 5b, the through-structure electronic substituent effect of the fluorinated groups lies within a straight correlation line, similar to a Hammett-type linear free-energy relationship.[18] This shows that favouring one catalytic parameter (*i.e.* lowering the overpotential) disfavours another one (*i.e.* TOF). In addition, careful positioning of through-structure substitution should be considered, as the addition of ester groups in the *meta*- or *ortho*-positions of the *meso* aryls in catalysts **6** and **7** can easily shift the overpotential, without significant differences in the catalytic rate.[37] A greater challenge in synthetic catalyst design is to escape these linear correlations and succeed in lowering the overpotential of the catalytic reaction while maintaining high TOF.

2.3. Bio-inspired catalyst modifications

One way of addressing the challenge of catalyst design is to take inspiration from natural systems which evolved over millions of years to perform efficient redox reactions at lower energetic costs. In nature, there are six pathways known to fix carbon dioxide as an organic material for biomass.[4] The dominant process is the reductive pentose phosphate (Calvin–Benson–Bassham) cycle which involves ribulose bisphosphate carboxylase/oxygenase (RuBisCO) catalysing the reaction of CO_2 with five-carbon sugar 1,5-ribulose bisphosphate to form two molecules of 3-phosphoglycerate (a precursor for a series of interconversions to form six-carbon sugar fructose-1,6-bisphosphate).[38] The other five pathways all involve net reactions of producing acetyl-CoA from CO_2 for anabolic (biosynthesis) and catabolic (energy) purposes: reductive acetyl-CoA pathway, reductive citric acid cycle, dicarboxylate/4-hydroxybutyrate cycle, 3-hydroxypropionate/4-hydroxybutyrate cycle, and 3-hydroxypropionate bi-cycle.[39]

Though the thermodynamically favourable direct reductions of CO_2 to methanol and methane are very important reactions, they are surprisingly not observed in natural systems, which instead use discrete two-electron reduction steps. For example, the Wood–Ljungdahl pathway for autotrophic growth and acetate synthesis involves initial two-electron reduction steps: the CO dehydrogenase (CODH)-catalysed reduction of CO_2 to CO and the formate dehydrogenase (FDH)-catalysed reduction of CO_2 to formate. Similar discrete two-electron steps are involved in the eight-electron reduction reactions observed for the methanogenic archaea catalysing reduction of CO_2 to methane and for the acetogenic bacteria catalysing reduction of CO_2 to acetic acid. The reasons for this strategy include (i) the versatility of these two-electron reduced intermediates to branch off into various pathways for the synthesis of cellular metabolites and (ii) the final products (*e.g.* methane and acetic acid) are usually just by-products in the overall energy conservation scheme.[40] As such, fundamental learning from the biological two-electron reduction of CO_2 to CO and formate would be particularly interesting in designing synthetic CO_2 reduction catalysts.

The active sites of these enzymes[4,41–45] are shown in Fig. 6 and they seemingly show similar features that could be starting points for bio-inspired design. First, they consist of sulphur-rich ligand structures (Fe_3S_4 clusters and pterin-like cofactors) that can store and supply electrons. Second, they show a substrate-activating environment by employing either a bifunctional Lewis acid–base pair or second coordination sphere activation by nearby amino acid residues. Third, they promote good CO_2 binding in meticulously pre-arranged active

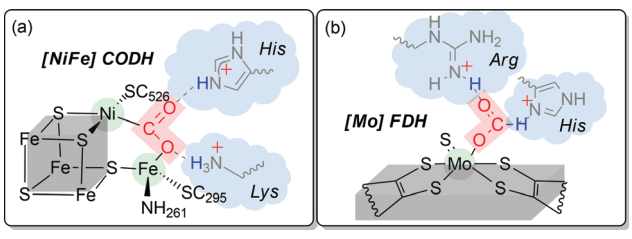

Fig. 6 CO_2-adduct intermediates found in the active site of (a) [NiFe]-centred carbon monoxide dehydrogenase (CODH) and (b) [Mo]-centred formate dehydrogenase (FDH) showing some common strategies for bio-inspired catalyst design.

sites with minimal changes in the geometry, resulting in low reorganizational energies (and consequently lower overpotentials). Lastly, they take leverage of the flexibility of their aqueous environment to manage proton supply, and promote proton-coupled electron transfer steps, significantly lowering the thermodynamic requirement of the reduction reactions.

Most bio-inspired approaches take into consideration these features by implementing a second coordination sphere effect for the known CO_2 reduction catalysts. The second coordination sphere relates to the distal structure of the catalyst beyond the primary coordination sphere of the ligand platform with the metal centre that may influence metal-bound intermediates and may or may not affect the electronic structure of the catalyst. Strategies relying on such effect have initially been extensively implemented in various synthetic catalysts for the reduction of dioxygen and protons, mimicking features observed in natural systems. Recently, this has been applied to the development of CO_2 reduction catalysts[18,46–48] and specific approaches can be generally categorized as follows: establishing local proton sources, tethering hydrogen bond relays, leveraging on cationic groups, and employing bimetallic structures.

2.3.1. Local proton source. The observation that the addition of weak Brønsted acids[26] enhances the catalytic reduction of CO_2 has already hinted the possibility of placing local acid proton sources in the periphery of the catalyst. This has been initially reported by the group of Savéant by placing eight pendant hydroxyl groups in FeTPP as shown in catalyst **9** (Fig. 7).[31] The introduction of these pendant proton donors resulted in enhanced CO_2-to-CO catalytic activity ($\log TOF_{max}$ = 5.97) at a lower overpotential (η' = 0.64 V) in DMF with 2 M H_2O (square markers in Fig. 7) compared with nonfunctionalized catalyst **1** under the same conditions ($\log TOF_{max}$ = 2.75 and η' = 0.74 V). The study also showed that replacing hydroxyl (–OH) groups with methoxy ($-OCH_3$) groups (catalyst **11**) results in a poorer activity ($\log TOF_{max}$ = 2.7) at a much larger overpotential (η' = 1.00 V).[16] In the presence of only one pendant hydroxyl group in catalyst **8**, the catalytic activity was significantly decreased ($\log TOF_{max}$ = 2.1 and η' = 0.91 V),[49] highlighting the crucial role of high local proton concentration in a push–pull (electron–proton) mechanism towards the metal carboxylate intermediate.[26]

The choice of the external proton source and the solvent is a critical factor for the activity of such type of catalyst. When using 3 M PhOH (circular markers in Fig. 7) instead of H_2O in DMF, the same catalyst **9** does not show significant improvements ($\log TOF_{max}$ = 3.8 and η' = 0.66 V) compared to catalyst **1** ($\log TOF_{max}$ = 4.5 and η' = 0.74 V).[32] Introducing 10 fluorine atoms as electron withdrawing groups in catalyst **10** slightly lowered the overpotential (η' = 0.59 V) but the activity ($\log TOF_{max}$ = 4.0) is still lower than that of catalyst **1**.[32] This implies that the pendant phenolic groups in catalysts **9** and **10** compete with the bulk concentrations of phenol in stabilizing the metal carboxylate intermediate. In the presence of H_2O as an external Brønsted acid, however, catalyst **9** shows a more local acidic environment directly interacting with the metal carboxylate intermediate. It is also noteworthy that when switching the solvent from the commonly used dimethylformamide (DMF) to acetonitrile (ACN), a significant improvement in the catalytic activity was observed for catalyst **8** ($\log TOF_{max}$ = 3.7) at a lower overpotential (η' = 0.78 V) in comparison with the same catalyst in DMF.[49] It was pointed out by the group of Warren that the unexpected solvent effect was due to the strong H-bond acceptor ability of DMF compared to ACN, disrupting the pre-established stabilization by the pendant phenolic groups.

The group of Nocera extended the investigation of the local proton source effect by establishing pendant phenolic and sulfonic groups in an iron hangman porphyrin configuration,[50] as shown in catalyst **12** and **13**, respectively (Fig. 7). The pendant –OH groups induced a thermodynamically favoured −5.0 kcal mol^{-1} stabilization of the CO_2 adduct. However, the introduction of sulfonic groups did not improve the catalytic activity of the system because once deprotonated, they cannot be reprotonated by the weaker external PhOH donor (the pK_a of sulfonic acid is 3 and the pK_a of PhOH is 18 in DMF[51]). The steric congestion and electrostatic repulsion from the negatively charged sulfonate group resulted in a mismatch of orientation in which the sulfonic group is no longer pointed towards the bound CO_2 substrate. This highlights the importance of the external acid source choice in regenerating the pendant local proton groups to maintain the second sphere coordination effect. The reference catalyst **14** lacking the hanging group showed similar activities to those of the modified iron hangman porphyrins, indicating that dibenzofuran clefts in **12** and **13** are not optimized to promote good CO_2 binding.

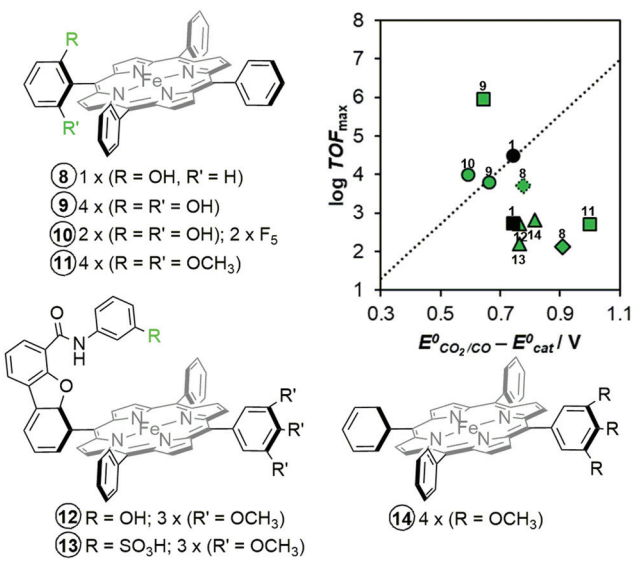

Fig. 7 Effect of functional groups acting as a local proton source in the second coordination sphere of modified iron porphyrins. Conditions: DMF with 3 M PhOH (circle) or 0.04 M PhOH (triangle) or 2 M H_2O (square) or 1 M H_2O (diamond); ACN with 1 M H_2O (dotted diamond). For relative comparison, the through-structure electronic scaling from Fig. 5b is shown as dotted line and the performance of the nonfunctionalized catalyst **1** is shown as black-shaded markers.

2.3.2. Hydrogen-bond donors. Another approach for the second coordination effect does not necessarily place local proton sources on the periphery of the catalyst, but places functional groups which are able to establish hydrogen bonding interactions (Fig. 8) either with the metal carboxylate adduct or with the external proton sources to synergistically stabilize the CO_2 reduction intermediates.

Placing one simple amine function in the *ortho* position of the *meso* aryl group in catalyst **15** slightly improved the catalytic activity ($\log TOF_{max}$ = 4.02) but with a slightly higher overpotential (η' = 0.76 V) as compared to the nonfunctionalized catalyst **1** under the same conditions ($\log TOF_{max}$ = 3.01, η' = 0.74 V).[52] However, placing this amino function in the *meta* position (catalyst **16**), increased the overpotential (η' = 0.82 V) but resulted in a lower catalytic activity ($\log TOF_{max}$ = 3.40). This indicates that even with the same functional group, a simple position modification can affect the catalytic properties of the system. It seems that the *ortho* positioning of the amino group is optimal for the stabilization of the metal carboxylate intermediate, having a DFT-calculated distance of 1.97 Å for (N)H···O(C). An iron hangman porphyrin with a guanidinium group (catalyst **17**) as a H-bond donor was reported by the group of Nocera and it showed a thermodynamically favoured −2.61 kcal mol^{-1} stabilization of the CO_2 adduct.[50] However, the catalytic activity was even poorer ($\log TOF_{max}$ = 2.47 and η' = 0.77 V) than that of the simple amino function, possibly because of the unoptimized dibenzofuran cleft preventing the guanidinium group from being at an appropriate distance with respect to the metal carboxylate intermediate, as was similarly reasoned for catalysts **12** and **13**.

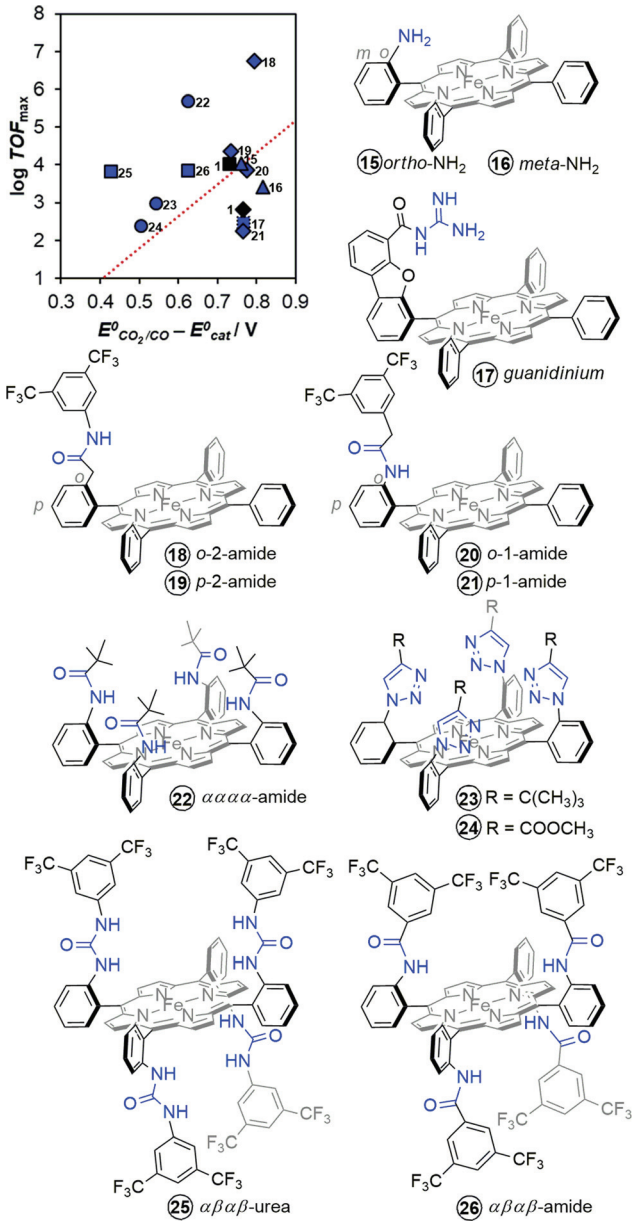

Fig. 8 Effect of functional groups acting as a hydrogen-bond relay in the second coordination sphere of modified iron porphyrins. Conditions: DMF with 1 M PhOH (triangle) or 0.1 M PhOH (diamond) or 0.04 M PhOH (dotted square) or 5 M H_2O (square; ACN with 3 M PhOH (circle). For relative comparison, the through-structure electronic scaling from Fig. 5b is shown as dotted line and the performance of the nonfunctionalized catalyst **1** is shown as black-shaded markers.

The group of Chang has systematically studied the importance of the position of amide moieties as hydrogen-bond donors in Fe-porphyrins (catalysts **18**, **19**, **20**, and **21**).[53] It was shown that the modified Fe-porphyrins with an *ortho* amide (catalysts **18** and **20**, $\log TOF_{max}$ = 4.35 to 6.74 and η' = 0.74 to 0.80 V) in the *meso* aryl of the porphyrin perform better than their corresponding analogues with a *para* configuration (catalysts **19** and **21**, $\log TOF_{max}$ = 2.23 to 3.84 and η' = 0.77 to 0.78 V). Furthermore, a distal position (catalyst **18**, $\log TOF_{max}$ = 6.74 and η' = 0.80 V) is better than a proximal one (catalyst **20**, $\log TOF_{max}$ = 4.35 and η' = 0.74 V).[53] This shows that proper positioning of the amide functions is critical to establishing suitable hydrogen bonding interactions with the metal carboxylate intermediate. They all improved the catalytic activity of the nonfunctionalized catalyst **1** but the overpotentials were still not significantly lower. Recently, the group of Dey has synthesized a picket fence iron porphyrin in an *αααα* atropoisomer configuration that contains proximal amides,[54] as shown in catalyst **22**. This catalyst has an improved catalytic rate ($\log TOF_{max}$ = 5.71) in ACN with 3 M PhOH while having a lower overpotential (η' = 0.62 V) as compared to those of catalysts with a single amide group (**18**, **19**, **20**, **21**). This shows that aside from proper positioning, the number of such pendant amido groups can also affect the catalytic activity of the system.

Our group has taken into account these subtleties and envisioned that employing urea groups (catalyst **25**) instead of amido groups would provide multiple-point hydrogen bonding stabilization of the metal carboxylate intermediate.[35] An *αβαβ* atropoisomer configuration was further considered to provide two sets of hydrogen bonding stabilization in a *trans* fashion towards the M-CO_2 intermediate, mimicking a similar configuration observed in the active site of CODH. This carefully designed catalyst significantly lowered the overpotential (η' = 0.43 V) while maintaining a good $\log TOF_{max}$ (3.83). A com-

parative study with an analogue catalyst containing amide groups as single-point hydrogen bond donors (catalyst **26**) resulted in a similar log TOF_{max} (3.85) but with a higher overpotential (η' = 0.63 V), underlying the importance of multi-point stabilization offered by the urea groups. A more detailed study based on the observations from the X-ray crystal structures of the catalysts and DFT calculations has revealed that indeed both N–H fragments of each urea arm show strong hydrogen bonding with the metal carboxylate intermediate with short (N)H···O(C) donor–acceptor distances of 1.76–1.88 Å (Fig. 9a). These distances are very similar to those reported for hydrogen bond distances between lysine and histidine residues and the CO_2 adduct in the active site of CODH (Fig. 6).

Kinetic and isotope-effect studies revealed that, unlike for previously described catalysts that require acidic proton sources (*e.g.* phenol and trifluoroethanol) for enhanced catalytic activity, water is a sufficient proton source for catalyst **25** and water molecules seem to work in synergy with the urea groups to provide higher catalytic activity. It was further evidenced by DFT calculations that a water molecule can be inserted between the M-CO_2 adduct and one urea arm with almost unchanged topology of the CO_2 intermediate (Fig. 9b). A similar strategy of trapping and leveraging water molecules in the triazole groups of catalysts **23** and **24** was utilized by the group of Dey to indirectly establish the stabilization of the CO_2 intermediate.[25,54] When compared to the catalyst bearing urea groups **25**, catalysts **23** and **24** showed a small effect on the overpotential (η' = 0.50 to 0.54 V) and catalytic activity (log TOF_{max} = 2.4 to 3.0). The aforementioned results reveal the importance of suitable H-bond donor positioning and number in the vicinity of the CO_2 intermediate to establish direct and efficient H-bonding stabilization that can improve the catalytic activity of the system. Unlike in the case of local proton sources, local H-bond donors can work in synergy with external proton sources to enhance the catalytic activity.

2.3.3. Cationic moieties. The observation that once the nearby amino acid residues in the active site of CODH are protonated, they establish a cationic environment that can stabilize the CO_2 intermediate (Fig. 6), hinted the possibility of tethering charged groups on the periphery of the iron porphyrin platform (Fig. 10). Indeed, substantial improvements

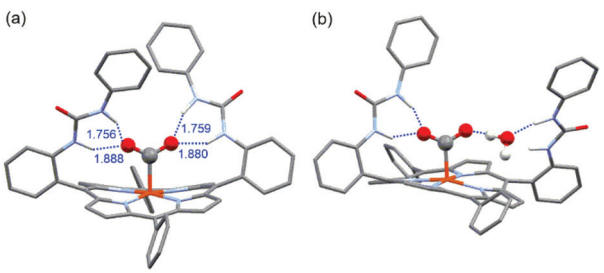

Fig. 9 DFT-optimized model structures of the (a) CO_2 intermediate with triply reduced catalyst **25** and (b) the synergistic stabilization in the presence of a water molecule.

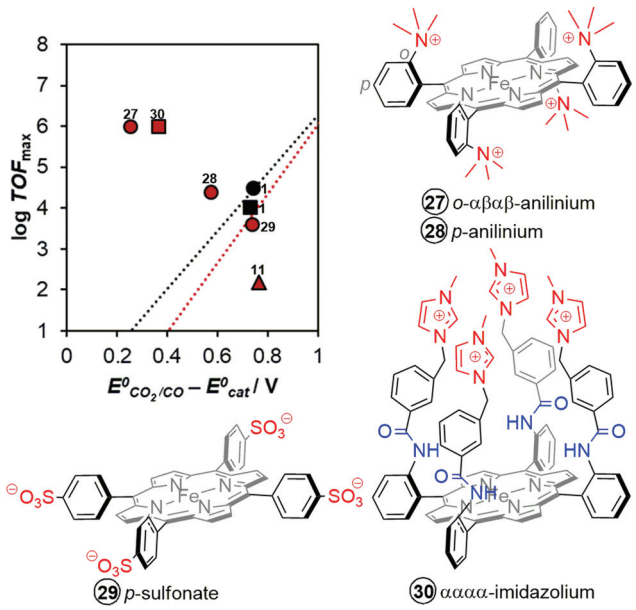

Fig. 10 Effect of charged functional groups in the second coordination sphere of modified iron porphyrins. Conditions: DMF with 3 M PhOH (circle) or 0.04 M PhOH (triangle) or 5 M H_2O (square). For relative comparison, the through-structure electronic scaling from Fig. 5b is shown as dotted line and the performance of the nonfunctionalized catalyst **1** is shown as black-shaded markers.

were observed with the incorporation of cationic functionalities like trimethylammonium groups (catalysts **27** and **28**) in iron porphyrin catalysts reported by the group of Robert, Costentin and Savéant.[34] The *ortho*-positioning (catalyst **27**) of these groups is optimal for through-space electrostatic interactions between the positive charges of substituents and the negative charge of the metal carboxylate intermediate and thus resulted in a significant decrease in the overpotential (η' = 0.25 V) with a simultaneous increase in the TOF (log TOF_{max} = 6).[18] Placing trimethylammonium groups in the *para* position led to catalyst (**28**) exhibiting a higher overpotential (η = 0.57 V) and lower catalytic activity (log TOF_{max} = 4.4), highlighting the importance of suitable orientation of these through-space electrostatic effects. A similar improvement was observed for the picket fence catalyst **30** containing the synergistic effects of cationic methylimidazolium groups and proximal amido groups acting as H-bond donors, resulting in a similarly improved catalytic performance (log TOF_{max} = 6 and η' = 0.37 V).[36]

Because of the cationic charges in these catalysts, they were also reported to have even higher catalytic performances in water as a solvent and proton source, which is a major advancement toward a more sustainable conversion of CO_2. Catalyst **28** shows high stability and catalytic activity in a quasi-neutral aqueous KCl solution (pH = 6.7) at an applied potential of −0.86 V *vs.* NHE. In a controlled potential electrolysis, the system maintains a faradaic efficiency higher than 98% for CO production over 72 h.[55] Recently, the same catalyst has also been reported by the group of Robert to photo-cataly-

tically reduce CO_2 to CH_4 when coupled to an Ir-based[56,57] or organic photosensitizer.[58] Catalyst **30** similarly showed good electrocatalytic activity and selectivity in water, resulting in 91% faradaic efficiency for CO production at −0.95 V *vs.* NHE. Although catalyst **27** shows the best performance so far in terms of $\log TOF_{max}$ and overpotential as shown in Fig. 10, there are no reported bulk electrocatalysis data in purely aqueous solution though it exhibited 100% faradaic efficiency over 84 h electrocatalysis in DMF solution containing 3 M PhOH and 0.1 M H_2O.[34]

The incorporation of negatively-charged sulfonate substituents (catalyst **29**), on the other hand, resulted in a decrease in the $\log TOF_{max}$ (3.6) and increase in the overpotential (η' = 0.74 V) as a result of electrostatic repulsions with the negatively charged metal carboxylate intermediate.[34] This was similarly observed for an iron hangman porphyrin containing sulfonic acid groups (catalyst **11**), which were immediately deprotonated in solution causing electrostatic repulsions of the sulfonate group away from the CO_2 intermediate.[50] These negative effects are clearly observed in the relative positioning of the performance of these catalysts towards the downward right part from the linear scaling as shown in Fig. 10.

2.3.4. Bimetallic design. Another approach for the secondary coordination effect is through the bimetallic approach which has been similarly observed in [NiFe]-centred CODH enzymes. The bimetallic system works cooperatively to store charges and to activate the CO_2 substrate in a classical push–pull donor–acceptor configuration. Naruta and co-workers developed a cofacial homobimetallic complex based on well-known CO_2-reducing iron porphyrin catalysts (Fig. 11).[59] Taking advantage of the rigidity of the porphyrin platforms and the modularity of a phenyl linker, they were able to control the distance between the two Fe metal centres. Compared to the monomeric catalyst **1**, a higher catalytic activity ($\log TOF_{max}$ = 4.3, faradaic efficiency = 95%, and η' = 0.71 V) was achieved with an *ortho* configuration of the dimer (catalyst **31**) where the Fe–Fe distance is expected to be 3.2–4.0 Å, suitable for the binding of the CO_2 substrate. Cyclic voltammetry studies show overlapping formal reductions of the two iron porphyrin catalysts, with the onset of the catalytic activity corresponding to the $Fe^{I/0}$ redox couple. The overpotential and catalytic activity of the system were further optimized using through-structure substituent effects (catalysts **32**, **33**, **34**, **35**, and **36**).[60] Introducing electron-withdrawing substituents into the phenyl rings of the porphyrin (catalyst **32**) lowered the catalytic reaction overpotential (η') to 0.56 V with a $\log TOF_{max}$ of 4.2. Introducing electron donating groups (catalyst **35**), on the other hand, resulted in a higher catalytic activity ($\log TOF_{max}$ = 5.8) at the cost of a higher overpotential (η' = 0.91 V).

2.4. Opportunities for future design modifications

Various synthetic routes to modify the iron tetraphenyl porphyrin platform has paved the way for several improvement strategies, as summarized in Fig. 12. The goal of all these strategies is to improve the overpotential and the catalytic turnover frequency of the system, without sacrificing the CO_2-to-CO selectivity and the faradaic efficiency of the parent catalyst. Through-structure substituent effects (black circles, Fig. 12) show a linear scaling relationship between the overpotential and the catalytic turnover frequency, where lower overpotentials are observed with electron-withdrawing groups (albeit with lower catalytic activities), and higher catalytic activities are achieved when electron-donating groups are introduced on the periphery of the catalyst (albeit with higher overpotentials). Second coordination sphere modifications can easily break away from this linear scaling relationship. Employing a bimetallic approach (orange circles, Fig. 12) with cofacial iron porphyrins slightly improves the catalytic activities but with no significant changes in the overpotentials, although the latter can easily be tuned by the classical through-structure electronic effects. Introducing local proton sources (green circles, Fig. 12) in the vicinity of the ligand framework initially showed great promise in improving the catalytic activity and to some

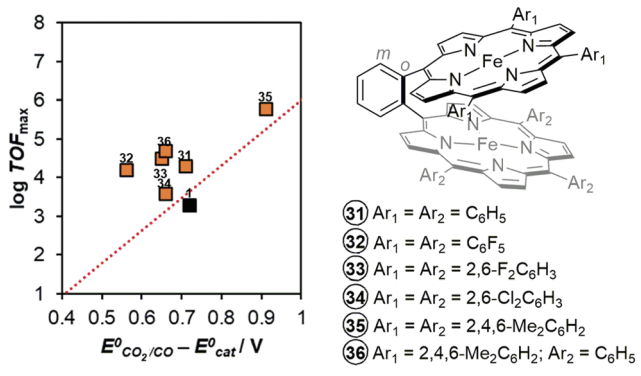

Fig. 11 Effect of bimetallic strategy in the second coordination sphere of modified iron porphyrins. Conditions: DMF with 5 M H_2O. For relative comparison, the through-structure electronic scaling from Fig. 5b is shown as dotted line and the performance of the nonfunctionalized catalyst **1** is shown as black-shaded marker.

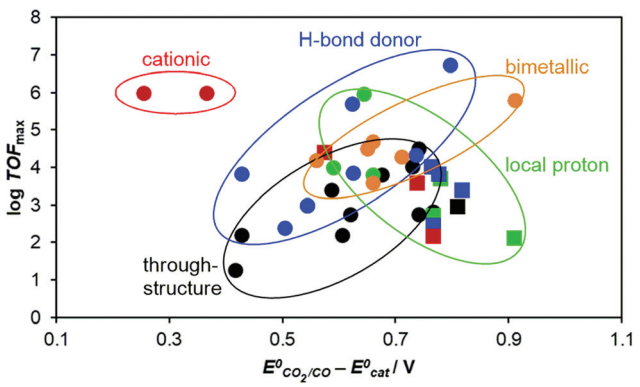

Fig. 12 Summary of the catalytic performances of iron porphyrins modified with various design strategies. (Circles represent the optimized effect while squares represent the unoptimized strategy due to improper positioning, number, and functional nature).

extent in lowering the overpotential, but a careful choice of catalytic conditions (solvent and proton source) is needed to ensure the introduction of proton-transfer and hydrogen bond-relay effects (unoptimized reinforcements shown in green squares). Tethering simple hydrogen bond donors, such as amino, amido, and urea functions (blue markers, Fig. 12), is another successful strategy because these functions seldom compete with external proton sources, and instead operate in synergy with the proton sources during the catalytic reaction. Great attention should also be paid to the proper positioning of the above-mentioned relays to maximize the performances of the catalyst (unoptimized reinforcement shown in blue squares). Lastly, it seems that significant improvements are observed when placing cationic moieties in the vicinity of the porphyrin platform (red markers) which significantly lowers the overpotential while improving the catalytic activity and further making it possible to perform the catalysis in water.

Though most of the studies presented here have focused on the modifications of the iron tetraphenylporphyrin, similar modifications can also be found in other porphyrin catalysts, though not as extensive (Fig. 13). Early studies of cobalt-based porphyrins with carboxylic acid (catalyst **37**) or sulfonic acid functions (catalyst **38**) in the *meso* aryl groups showed the electrocatalytic reduction of CO_2 to formic acid in aqueous solutions, though the products were not quantified.[19] A cobalt tetraphenyl porphyrin (CoTPP, catalyst **39**) was similarly reported to show enhanced catalytic currents under CO_2 with the onset of catalytic current occurring at the $Co^{I}TPP/Co^{0}TPP$ redox couple (−2.02 V *vs.* SCE in butyronitrile solution), however controlled electrolysis and identification of products were not pursued.[61] Interestingly, a cofacial metalloporphyrin was self-assembled using electrostatic interactions between a cationic Co-5,10,15,20-tetrakis(4-methylpyridyl)porphyrin and an anionic Co-5,10,15,20-tetrakis(4-sulfonatophenyl)porphyrin (catalyst **43**), and it showed catalytic CO_2 reduction activity at −1.80 V *vs.* Ag/Ag^+, forming CO and formaldehyde, with traces of H_2.[62] This activity was attributed presumably to Co(I) of the cationic porphyrin as the anionic counterpart only acted as an electron mediator. Changing the metal ion of the electron mediator with a Cu (a mixed Co–Cu complex in catalyst **44**) resulted in higher catalytic current densities.

Aside from varying the nature of the central metal ion, a recent study by the group of Welch has also been reported on thienyl-substituted porphyrins (catalyst **40** and **41**), dispensing with the usual *meso* aryl groups. Compared to iron tetraphenylporphyrins (**1**), both catalysts operate at a 150 mV lower overpotential, which is attributed to the extension of the π-conjugation in thienyl-porphyrins, wherein the stabilizing mesomeric effects overcome any destabilizing inductive effects associated with the thiophene being more electron-rich than the phenyl groups.[63] The catalytic activity is slightly lower than that of **1** with a $\log TOF_{max}$ = 3.78 for catalyst **40** and a $\log TOF_{max}$ = 3.45 for catalyst **41**. Interestingly, controlled potential electrolysis showed a lower TON = 10 for catalyst **40** due to the oxidative electropolymerization of thiophene units on the counter electrode, a phenomenon that can be perceived to be useful in surface immobilization of the catalyst (see the next chapter on heterogenous catalysis). This degradation process was prevented by protecting the vulnerable position of thiophene units by a methyl group in catalyst **41**, resulting in a three-fold increase in TON. Recently, the group of Dey has also reported an iron porphyrin catalyst bearing four ferrocene moieties (catalyst **42**) that made it possible to reduce CO_2 to CO in the presence of dioxygen.[64] The dioxygen tolerant activity stems from (i) the role of ferrocene groups acting as a redox fuse for the reduction of dioxygen to benign water, and (ii) the intrinsic 500 times faster rate of reaction of the Fe^0 active form of the catalyst towards CO_2 substrates as compared to O_2 substrates, even though the latter has a higher driving force. All these recent developments point to many opportunities and avenues in catalyst design improvement for such a tuneable and efficient porphyrin platform towards CO_2 reduction.

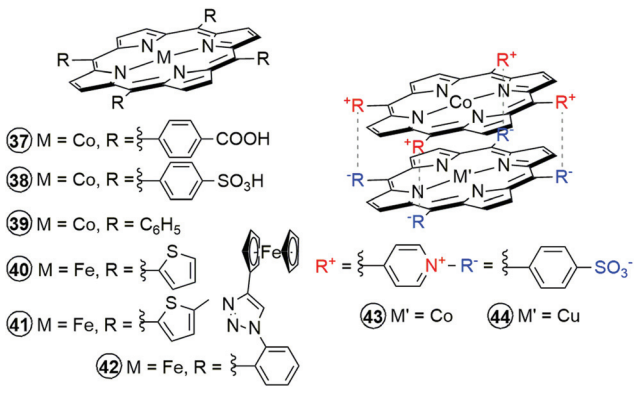

Fig. 13 Other modifications of metalloporphyrin-based molecular catalysts for CO_2 reduction, showing future opportunities for catalyst improvement.

3. Heterogenous CO_2 reduction

Homogenous catalysis offers two main advantages. The first is the relative ease to tune synthetically the structure and therefore the physical properties of the catalyst in order to modulate the performances of the catalytic system, and the second is the better compatibility of the homogenous conditions with the different spectroscopic methods employed to detect and characterize reactive intermediates, which facilitates the elucidation of the mechanistic details of the catalytic reaction. As mentioned earlier, metalloporphyrin catalysts for CO_2 reduction were mainly studied in the context of molecular electrocatalysis. However, homogeneous catalysts present in the electrolyte can only be electro-activated in the first diffusion layer on the surface of the cathode. Heterogeneous molecular electrocatalysis offers the possibility of overcoming this and other drawbacks such as slow multielectron transfer steps to

the catalyst often associated with molecular homogeneous electrocatalysis. Immobilizing the molecular catalysts on the surface of an electrode for heterogeneous molecular electrocatalysis may circumvent these intrinsic limitations as compared to homogeneous studies.[65] Heterogenization also permits the transfer of the electrons in solvents such as water that otherwise could not be employed because of the low solubility of metalloporphyrins in aqueous medium.[65–74] An important aspect to bear in mind for the development of electrolysers that can couple, for example, CO_2 reduction with water oxidation to dioxygen,[75] is the compartmentalization of the cathodic and anodic processes. The immobilization of molecular CO_2 reduction catalysts on the cathode or water oxidizing catalysts on the anode is currently investigated to develop chemically modified cathodes and anodes.

Unlike in heterogeneous catalysis performed on the surface of catalytically active materials such as metal oxides or alloys, this heterogeneous approach uses conductive but catalytically inactive surfaces to immobilize catalytically active molecular catalysts. Carbon-based electrodes including glassy carbon (GC) electrodes, activated carbon fibers (ACF), gas diffusion electrodes (GDE), carbon paper, pyrolitic graphite (PG) electrodes, and carbon fabric electrodes are especially suitable as a cathode for the immobilization of molecular CO_2 reduction catalysts because of their high overpotential for competing hydrogen production and their stability under reducing conditions. Since the first report by the group of Aramata on the catalytic CO_2 reduction by a CoTPP fixed on a glassy carbon electrode through a 4-aminopiridine linker,[76] several examples of heterogeneous electrocatalytic systems based on the immobilization of metalloporphyrins, almost exclusively on carbon-based electrodes, have been reported. Here we will present a brief overview of the different methods developed to prepare these modified electrodes and their catalytic activity towards CO_2 reduction.

3.1. Electrode modification by adsorption

Chemisorption is certainly the most convenient and straightforward technique to immobilize metalloporphyrins on the surface of carbonaceous electrodes. The spontaneous non-covalent modification of the electrode surface stems from the strong affinity of the delocalized π conjugated systems of these macrocycles. These modified electrodes were shown to be stable enough for long periods in a solvent in which the catalyst is not soluble. The group of Sakata reported in 1999 the electrochemical reduction of CO_2 at Co-, Fe-, Ni-, Zn- and Cu-TPP supported gas diffusion electrodes (GDE) under high pressure of CO_2.[66] An average of 6×10^{-8} mol cm^{-2} catalyst surface concentration on the GDE was obtained by impregnation of the electrode using a dichloromethane solution of different catalysts. Under 20 atm pressure of CO_2 all these catalysts produced a mixture of CO, H_2, and HCOOH but only Co- and Fe-TPP were able to reach over 80% faradaic efficiency for CO_2 reduction and over 80% selectivity for CO production. It was reported later that combining the GDE and activated carbon fibers to immobilize Co-5,10,15,20-tetrakis(4-methoxyphenyl)-porphyrin (**45**, Fig. 14) can increase significantly the catalyst concentration on the electrode to reach a current density as high as 50–70 mA cm^{-2} for CO production with over 85% selectivity at atmospheric CO_2 pressure.

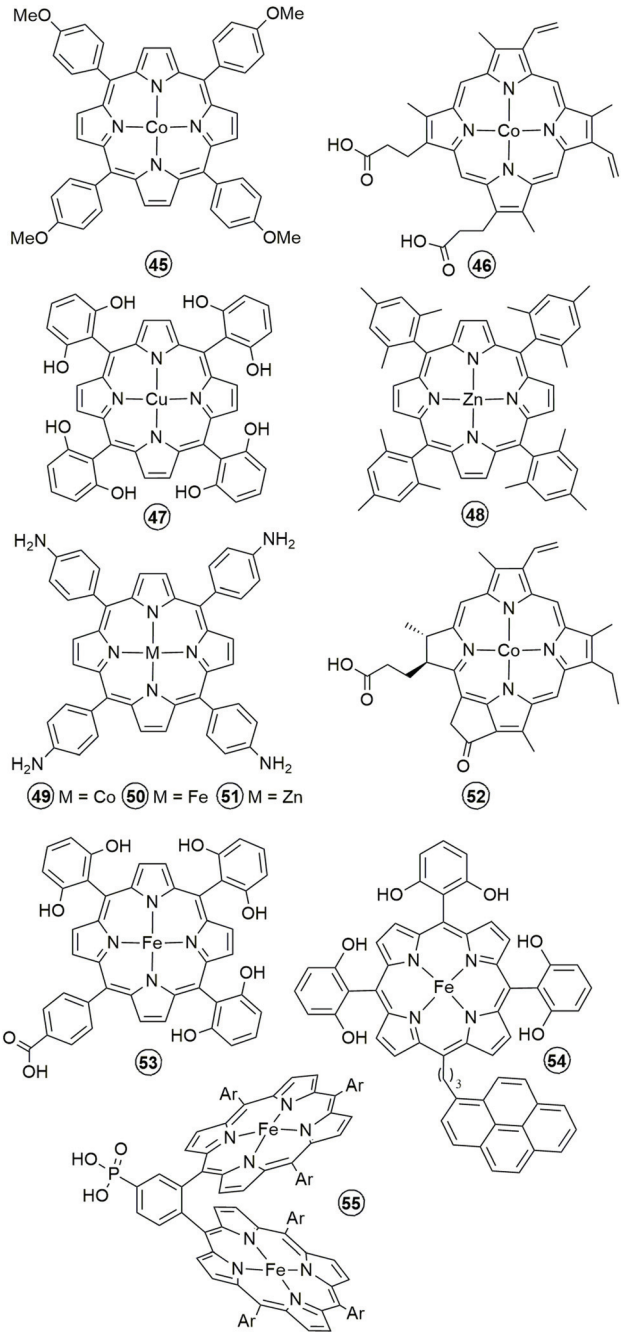

Fig. 14 Metalloporphyrins used in the preparation of modified cathodes for the heterogeneous electrocatalytic reduction of CO_2.

Using pyrolitic graphite (PG) electrodes to dock Co-protoporphyrin catalysts (**46**, Fig. 14), the group of Koper reported the electrochemical reduction of CO_2 in acidic aqueous media (pH 1–3) to produce CO with current densities of 0.08 and 0.16 mA cm^{-2} for 1 h, corresponding to TOFs of *ca.* 0.2 and

0.8 s^{-1}.[77] More importantly, under these acidic conditions, a small amount of methane and trace amounts of HCOOH and methanol were detected.

A remarkably higher production of multi-electron reduction was later reported by the groups of Brudvig and Wang using chemisorbed Cu-5,10,15,20-tetrakis(2,6-dihydroxyphenyl)-porphyrin (**47**, Fig. 14) on carbon nanoparticle coated carbon fiber paper.[67] At −0.976 V *vs.* NHE, in addition to CO, the catalyst was able to drive partial current densities of 13.2 and 8.4 mA cm^{-2}, corresponding to TOFs of 3.4 and 1.8 site^{-1} s^{-1} for methane and ethylene production from CO_2 reduction corresponding to a faradaic efficiency of 44% for these two products. Using the same technique to immobilize Zn-5,10,15,20-tetrakis-mesitylporphyrin (**48**, Fig. 14), these authors have argued that the electrocatalytic reduction of CO_2 originated from the non-innocent electrochemical reactivity of the porphyrinic ligand.[68] In fact, despite the redox-inactivity of zinc within the potential window of the catalysis, CO was produced with a faradaic efficiency of 95% at −1.7 V *vs.* SHE and a TOF as high as 14 site^{-1} s^{-1}.

3.2. Electrode modification by electropolymerization

By introducing the appropriate groups on the periphery of the porphyrin macrocycle, the corresponding catalyst can be easily supported on an electrode using electropolymerization. Co-, Fe- and Zn-5,10,15,20-tetrakis(4-aminophenyl)porphyrins (**49**, **50**, and **51**, Fig. 14) were used by the group of Issacs in potentiodynamic cycles to grow polymeric films on an ITO electrode.[78,79] The electrocatalytic properties toward CO_2 reduction of these three catalysts were evaluated in a $BMImBF_4$ (1-butyl-3-methylimidazolium tetrafluoroborate) ionic liquid as a novel electrolyte for CO_2 electroreduction. All catalysts produced CO at particularly lower overpotentials, −0.8 V *vs.* Ag/AgCl, but while the electropolymerized Co- and Fe-porphyrins exhibited 67% and 78% faradaic efficiency, respectively, the corresponding Zn-based catalyst shows only 15% faradaic efficiency.

3.3. Electrode modification using multi-walled carbon nanotubes and Nafion® membrane

A combination of multi-walled carbon nanotubes (MWCNTs) and Nafion® has recently emerged as another technique of choice for the rapid preparation of modified electrodes with molecular catalysts of high surface areas.[69,75,80,81] The Nafion® polymeric membrane holds the molecular catalyst-impregnated MWCNTs attached to the surface of the electrode while offering high proton permeability and effective access of the substrate (CO_2) to the membrane-catalyst-electrode layers where the electrochemical reaction takes place. The molecular catalyst can be mechanically (*e.g.* ultrasound mixing in a solution of the catalyst) or covalently introduced in the MWCNTs. Using the first method, Fukuzumi and coworkers prepared a glassy carbon modified electrode by drop casting a sonicated acetonitrile solution containing Co-chlorin (**52**, Fig. 14), MWCNTs and Nafion®.[69] CO and H_2 were produced using this modified electrode in an aqueous buffer (pH = 4.6) solution at −1.1 V *vs.* NHE with 89% and 11% faradaic efficiencies, respectively. The catalysis reaches a maximum TON of 1100 and TOF of 2.3 site^{-1} s^{-1}. A pyrene-appended Fe-porphyrin bearing six pendant OH groups on the phenyl rings in all *ortho* and *ortho′* positions (**54**, Fig. 14) was also immobilized on carbon nanotubes *via* noncovalent interactions and further deposited on the glassy carbon electrode.[82] The obtained carbon material had an active-catalyst surface concentration of 2.4 × 10^{-8} mol cm^{-2} and exhibited highly selective and rapid electroreduction of CO_2 to CO in water (pH 7.3) at −1.03 V *vs.* NHE. The catalysis could be sustained for more than 3 hours with 97% total faradaic efficiency and 96% selectivity for CO production with a TON = 480 and a TOF = 0.4 site^{-1} s^{-1}. By using a similar procedure, Fe-5,10,15,20-tetrakis(4-(trimethylamino)-phenyl)-porphyrin (**28**, Fig. 10) was incorporated into a carbon paper-based cathode in a complete electrochemical cell, coupling CO_2 reduction to water oxidation.[75] The analysis of electrolysis products at a cathodic potential of −0.86 V *vs.* NHE for several hours in quasi-neutral water showed faradaic efficiencies of 90% for CO along with 10% for H_2 in the cathodic compartment and 99% for O_2 in the anodic compartment. In two different studies by the groups of Robert[80] and Han,[81] the covalent attachment of Fe- or Co-porphyrin (**53** and **46** respectively in Fig. 14) catalysts with the MWCNTs was reported to improve significantly the long-term stability of the catalysts while maintaining a good selectivity for CO production at reasonably lower overpotentials.

Even in the absence of the Nafion® membrane, the group of Daasbjerg reported enhanced catalytic activity and selectivity (>90%) for CoTPP (**39**), as compared to the homogenous catalysis, upon straightforward immobilization onto carbon nanotubes and adsorption on glassy carbon.[70] The electrode has a relatively high catalyst loading of 1.7 × 10^{-7} mol cm^{-2} and can be stable for over 4 h in bulk electrolysis mode at −1.35 *vs.* SCE with a current density of 3.2 mA cm^{-2}, a TON of 1118 and a TOF of 0.78 site^{-1} s^{-1}. An organic cage composed of six FeTPPs (**1**) was also immobilized on the MWCNT present on the surface of a glassy carbon electrode without the use of Nafion®, as reported by the group of Chang.[71] This electrode exhibited a higher porosity than a similar electrode prepared using a simple FeTPP. It has an active iron center concentration of 3.7 mol cm^{-2} and over 54% of the iron center was active compared to only 38% for the latter. The electrocatalytic reduction of CO_2 using this electrode in aqueous solution (pH = 7.3) produced CO exclusively at −0.63 *vs.* The RHE showed a higher TON = 55 205 and TOF = 0.64 site^{-1} s^{-1} in 24 h than the FeTPP-based electrode (TON = 32 770 and TOF = 0.38 site^{-1} s^{-1}). The difference in the catalytic performance between the two electrodes was attributed to the greater exposure of iron sites observed in the porphyrin–cage based catalyst and the potentially greater diffusion and local concentration of CO_2 in the hydrophobic cavity. This is due to a better diffusion of the substrate and the electrolyte throughout an array of readily accessible catalytic metal centers as opposed to the aggregation of planar FeTPP molecules that can diminish the number of electrochemically accessible and active metal centers.

3.4. Covalent modification of the electrode

The functionalization of an electrode surface by means of covalent chemical bond formation was first attempted by the group of Aramata.[76] A glassy carbon electrode was first functionalized using a 4-aminopyridine group and then Co-5,10,15,20-tetrakis(4-carboxyphenyl)porphyrin (**37**, Fig. 13) was fixed through the coordination of the pyridine on Co. The modified electrode showed a catalyst surface concentration of 10^{-12} mol cm^{-2} and was able to produce CO with 50% faradaic efficiency at −1.2 V *vs.* SCE in a CO_2-saturated standard phosphate buffer solution (pH = 7). Despite this result, some questions still persist about the stability of the Co-pyridine bond in the active, reduced and electron-rich form of the catalyst and about the catalyst role that pyridine itself can play in the electrocatalytic reduction of CO_2.[72]

Recently, a "click" azide–alkyne cycloaddition reaction has been employed to directly and covalently attach acetylene groups bearing Co-porphyrin to an azide functionalized boron-doped, p-type conductive diamond electrode (Fig. 15).[83] The obtained "smart" electrode has 6.33×10^{-11} mol cm^{-2} catalyst coverage and was used for the electrocatalytic reduction of CO_2, exhibiting good stability for over 1000 cycles in the cyclic voltammetry mode with CO being the main product of the reaction. Naruta and coworkers also reported the covalent grafting of a cofacial bimetalic Fe-porphyrin complex (**55**, Fig. 14) as CO_2 reduction catalyst on SnO_2 or TiO_2 coated fluorine-doped tin oxide (FTO) cathode.[84] The modified electrode has up to 4.7×10^{-12} mol cm^{-2} areal catalyst concentration and can reduce CO_2 to CO in nonaqueous (DMF or ACN) and aqueous solutions. For example, CO was obtained with a 90% faradaic efficiency in neutral water at −0.95 V *vs.* NHE in a 6 h electrolysis experiment.

3.5. Electrode modification by metal organic frameworks (MOFs) or covalent organic frameworks (COFs)

In both homogenous and heterogeneous catalysis, the first step of the electrocatalytic CO_2 reduction by metalloporphyrins is the electron transfer from the cathode to the catalyst, generating the reduced active form, which in turn reacts chemically with CO_2 leading eventually to the reaction products. The overall rate of the catalytic reaction, represented by the current density, is governed by both the rate of the reaction between the CO_2 and the active species, and the concentration of these species.[85,86] Unlike in homogenous catalysis, in a heterogeneous system, where the molecular catalyst is immobilized on the electrode surface, the catalysis is not limited by catalyst solubility or its diffusion rate toward the electrode. Thus, higher overall rates for the electrocatalytic reaction at a given applied potential can be achieved by increasing the areal concentration of active catalyst on the electrode.[86] Of note, limitations in the design of chemically-modified electrodes by impregnation reside in the determination of the number of active sites and also the variability of the active sites owing to partial chemical alteration of the initial catalyst.

Metal–organic framework (MOF) thin films were used to increase the areal concentration of metalloporphyrin catalysts on working electrodes for CO_2 reduction.[87,88] In contrast to a densely packed polymerized film, a MOF creates an ordered, porous heterogeneous network, which allows for free permeation of electrolyte counter ions and dissolved CO_2 into the interior of the film. For example, a thin film of Fe-porphyrin based MOF was employed as a platform for anchoring a substantial quantity of the molecular catalyst on a FTO conductive electrode for the electrochemical reduction of CO_2 (Fig. 16).[87] The measured surface concentration of the active catalyst (6.2×10^{-8} mol cm^{-2}) was reported to be much higher than that of the estimated fully packed single layer on a flat surface (7×10^{-11} mol cm^{-2}). Quasi equal amounts of CO and H_2 were produced using this modified electrode with ~100% faradaic efficiency at −1.3 V *vs.* NHE with a current density of 5.9 mA cm^{-2} for ~3.5 h (TON = 1520 and TOF = 0.13 site^{-1} s^{-1} for CO production) in 1 M trifluoroethanol solution in DMF. Immobilized Co-porphyrin based MOF, exhibiting a 1.1×10^{-7} mol cm^{-2} areal active-catalyst concentration, was also reported to reduce CO_2 in an aqueous solution at −0.7 V *vs.* NHE to produce CO in excess of 76% with a current density of 5.9 mA cm^{-2}.[88] The per-site TON obtained for 7 h electrolysis was 1400 which correspond to a TOF of 0.56 site^{-1} s^{-1}.

Covalent organic frameworks (COFs) comprising Co-porphyrin catalyst were also deposited as microcrystalline powder on a carbon fabric electrode for electrochemical CO_2 reduction.[89] Despite the high porosity and dispersion of Co centers on the electrode, it suffered a low active site ratio, with only 4% of the total catalyst on the surface, due to aggregation. Nevertheless, this electrode showed exceptional stability for 24 h and higher selectivity (90%) and TON (up to 290 000), with initial *TOF* of 26.1 site^{-1} s^{-1} for CO production at low applied potentials (0.65 V *vs.* NHE) in neutral water.

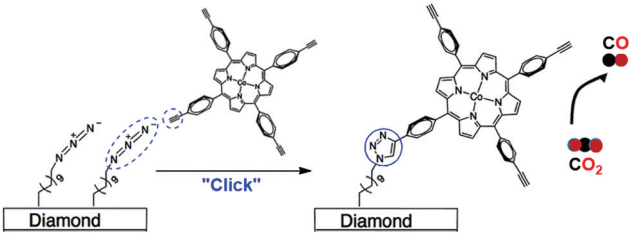

Fig. 15 Covalent modification of a diamond cathode surface for the heterogeneous electrocatalytic CO_2 reduction. Adapted with permission from ref. 83.

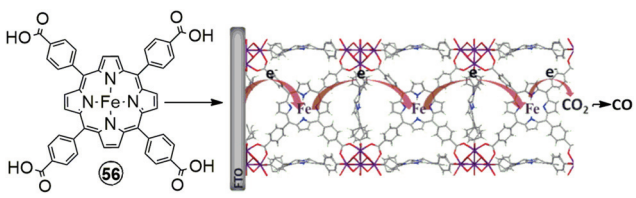

Fig. 16 Fe-porphyrin based metal–organic frameworks (MOFs) for the modification of cathodes in the heterogeneous electrocatalytic CO_2 reduction. Adapted with permission from ref. 87.

As demonstrated by these last three examples of modified electrodes, MOFs and COFs utilization can increase significantly the areal active-catalyst concentration and thus the catalytic current density. However, a decrease in the catalytic activity can be observed for a higher active-site loading due to charge-transport limitation from the electrode to the periphery of MOFs or COFs as the thickness of the film increases. To overcome this limitation, the group of Chang electronically tuned a two-dimensional COF by modification of the reticular structure.[90] Improved charge transport along the COF backbone was observed, promoting better electronic connectivity between remote functional groups and the active sites, and enabling the modulation of the catalytic properties of the system.

4. Conclusions and perspectives

As it transpires from these studies, the porphyrin macrocycle, also termed the pigment of life,[91] has been a solid brick to construct an excellent molecular component for chemists to activate and reduce CO_2 to various reduced forms of carbon. Their implementation in the design of chemically modified electrodes is already resulting in highly active materials. Fe-porphyrin supported on carbonaceous surface has been already tested in a lab design electrochemical cell where the reduction of CO_2 has been successfully coupled to the water oxidation reaction with exalting global yield.[75] Their cobalt phthalocyanine congener (another tetrapyrrolic macrocycle not surveyed in this review) was found to rival referenced Ag and Au nanoparticles for the CO_2-to-CO reduction in a similar complete electrolysis cell,[92] with recent studies even showing great promise for CO_2-to-methanol reduction.[93,94] With such breakthroughs, we can reasonably argue that the decisive focus on molecular catalysis has opened new avenues in this field. One important facet of molecular catalysis is the ability to decipher the intimate steps in the activation of small molecules such as CO_2. We can expect in the near future to capture different intermediates to underpin the mechanistic routes that would furthermore help to conduct higher desired selectivity in the CO_2 reduction. The development of multimetallic catalysts that can synergistically provide multiple electrons to CO_2 should lead to reduced forms of carbon. A particular challenge will be to guide the formation of carbon–carbon bonds for the production of higher carbon containing energy rich compounds. The reactivity routes of molecular catalysts at the surface of electrodes are not an extension of the ones observed in homogeneous medium. The understanding of the enhancement or decrease of surface catalytic activities must be comprehended to provide a rationale for the preparation of optimized chemically modified electrodes. We make no mistake in saying that dedicated research at the frontiers between fundamental and applied research must be encouraged with the aim of providing rapid solutions to tackle this urgent issue.

Conflicts of interest

There are no conflicts to declare.

Acknowledgements

This work was supported by the CEA IRTELIS PhD fellowship program (for Dr P. Gotico), LabEx CHARMMMAT, and by the French Infrastructure for Integrated Structural Biology (FRISBI) ANR-10-INSB-05-01.

References

1 R. K. Pachauri and L. A. Meyer, Climate Change 2014: Synthesis Report, Intergovernmental Panel on Climate Change, Geneva, Switzerland, 2014.
2 C. Ampelli, S. Perathoner and G. Centi, *Philos. Trans. R. Soc., A*, 2015, **373**, 20140177.
3 C. Hepburn, E. Adlen, J. Beddington, E. A. Carter, S. Fuss, N. M. Dowell, J. C. Minx, P. Smith and C. K. Williams, *Nature*, 2019, **575**, 87–97.
4 A. M. Appel, J. E. Bercaw, A. B. Bocarsly, H. Dobbek, D. L. DuBois, M. Dupuis, J. G. Ferry, E. Fujita, R. Hille, P. J. A. Kenis, C. A. Kerfeld, R. H. Morris, C. H. F. Peden, A. R. Portis, S. W. Ragsdale, T. B. Rauchfuss, J. N. H. Reek, L. C. Seefeldt, R. K. Thauer and G. L. Waldrop, *Chem. Rev.*, 2013, **113**, 6621–6658.
5 J.-M. Savéant, *Chem. Rev.*, 2008, **108**, 2348–2378.
6 N. Elgrishi, M. B. Chambers, X. Wang and M. Fontecave, *Chem. Soc. Rev.*, 2017, **46**, 761–796.
7 H. Takeda, C. Cometto, O. Ishitani and M. Robert, *ACS Catal.*, 2017, **7**, 70–88.
8 A. Glüer and S. Schneider, *J. Organomet. Chem.*, 2018, **861**, 159–173.
9 R. Francke, B. Schille and M. Roemelt, *Chem. Rev.*, 2018, **118**, 4631–4701.
10 C. Jiang, A. W. Nichols and C. W. Machan, *Dalton Trans.*, 2019, **48**, 9454–9468.
11 F. Franco, S. Fernández and J. Lloret-Fillol, *Curr. Opin. Electrochem.*, 2019, **15**, 109–117.
12 K. E. Dalle, J. Warnan, J. J. Leung, B. Reuillard, I. S. Karmel and E. Reisner, *Chem. Rev.*, 2019, **119**, 2752–2875.
13 E. Anxolabéhère-Mallart, J. Bonin, C. Fave and M. Robert, *Dalton Trans.*, 2019, **48**, 5869–5878.
14 F. A. Walker and U. Simonis, *Encyclopedia of Inorganic Chemistry*, American Cancer Society, 2006.
15 C. Costentin, S. Drouet, M. Robert and J.-M. Savéant, *J. Am. Chem. Soc.*, 2012, **134**, 11235–11242.
16 C. Costentin, M. Robert and J.-M. Savéant, *Chem. Soc. Rev.*, 2013, **42**, 2423–2436.
17 C. Costentin and J.-M. Savéant, *ChemElectroChem*, 2014, **1**, 1226–1236.
18 C. Costentin and J.-M. Savéant, *Nat. Rev. Chem.*, 2017, **1**, 0087.
19 K. Takahashi, K. Hiratsuka, H. Sasaki and S. Toshima, *Chem. Lett.*, 1979, **8**, 305–308.
20 M. Hammouche, D. Lexa, J. M. Savéant and M. Momenteau, *J. Electroanal. Chem. Interfacial Electrochem.*, 1988, **249**, 347–351.

21 C. Römelt, J. Song, M. Tarrago, J. A. Rees, M. van Gastel, T. Weyhermüller, S. DeBeer, E. Bill, F. Neese and S. Ye, *Inorg. Chem.*, 2017, **56**, 4745–4750.
22 C. Römelt, S. Ye, E. Bill, T. Weyhermüller, M. van Gastel and F. Neese, *Inorg. Chem.*, 2018, **57**, 2141–2148.
23 A. J. Morris, G. J. Meyer and E. Fujita, *Acc. Chem. Res.*, 2009, **42**, 1983–1994.
24 J. Schneider, H. Jia, J. T. Muckerman and E. Fujita, *Chem. Soc. Rev.*, 2012, **41**, 2036–2051.
25 B. Mondal, A. Rana, P. Sen and A. Dey, *J. Am. Chem. Soc.*, 2015, **137**, 11214–11217.
26 C. Costentin, S. Drouet, G. Passard, M. Robert and J.-M. Savéant, *J. Am. Chem. Soc.*, 2013, **135**, 9023–9031.
27 M. Hammouche, D. Lexa, M. Momenteau and J. M. Saveant, *J. Am. Chem. Soc.*, 1991, **113**, 8455–8466.
28 I. Bhugun, D. Lexa and J.-M. Saveant, *J. Am. Chem. Soc.*, 1994, **116**, 5015–5016.
29 I. Bhugun, D. Lexa and J.-M. Savéant, *J. Am. Chem. Soc.*, 1996, **118**, 1769–1776.
30 C. Costentin, M. Robert and J.-M. Savéant, *Acc. Chem. Res.*, 2015, **48**, 2996–3006.
31 C. Costentin, S. Drouet, M. Robert and J.-M. Savéant, *Science*, 2012, **338**, 90–94.
32 C. Costentin, G. Passard, M. Robert and J.-M. Savéant, *Proc. Natl. Acad. Sci. U. S. A.*, 2014, **111**, 14990–14994.
33 I. Azcarate, C. Costentin, M. Robert and J.-M. Savéant, *J. Phys. Chem. C*, 2016, **120**, 28951–28960.
34 I. Azcarate, C. Costentin, M. Robert and J.-M. Savéant, *J. Am. Chem. Soc.*, 2016, **138**, 16639–16644.
35 P. Gotico, B. Boitrel, R. Guillot, M. Sircoglou, A. Quaranta, Z. Halime, W. Leibl and A. Aukauloo, *Angew. Chem., Int. Ed.*, 2019, **58**, 4504–4509.
36 A. Khadhraoui, P. Gotico, B. Boitrel, W. Leibl, Z. Halime and A. Aukauloo, *Chem. Commun.*, 2018, **54**, 11630–11633.
37 R. B. Ambre, Q. Daniel, T. Fan, H. Chen, B. Zhang, L. Wang, M. S. G. Ahlquist, L. Duan and L. Sun, *Chem. Commun.*, 2016, **52**, 14478–14481.
38 J. A. Bassham, A. A. Benson and M. Calvin, *J. Biol. Chem.*, 1950, **185**, 781–787.
39 G. Fuchs, *Annu. Rev. Microbiol.*, 2011, **65**, 631–658.
40 M. Can, F. A. Armstrong and S. W. Ragsdale, *Chem. Rev.*, 2014, **114**, 4149–4174.
41 H. Dobbek, V. Svetlitchnyi, L. Gremer, R. Huber and O. Meyer, *Science*, 2001, **293**, 1281–1285.
42 J.-H. Jeoung and H. Dobbek, *Science*, 2007, **318**, 1461.
43 J. Fesseler, J.-H. Jeoung and H. Dobbek, *Angew. Chem., Int. Ed.*, 2015, **54**, 8560–8564.
44 T. Reda, C. M. Plugge, N. J. Abram and J. Hirst, *Proc. Natl. Acad. Sci. U. S. A.*, 2008, **105**, 10654–10658.
45 H. Dobbek, *Coord. Chem. Rev.*, 2011, **255**, 1104–1116.
46 Y. Matsubara, *ACS Energy Lett.*, 2019, 1999–2004.
47 J. M. Le and K. L. Bren, *ACS Energy Lett.*, 2019, 2168–2180.
48 A. W. Nichols and C. W. Machan, *Front. Chem.*, 2019, **7**, 397.
49 S. Sinha and J. J. Warren, *Inorg. Chem.*, 2018, **57**, 12650–12656.
50 C. G. Margarit, C. Schnedermann, N. G. Asimow and D. G. Nocera, *Organometallics*, 2019, **38**, 1219–1223.
51 A. J. Libbey and J. T. Stock, *Anal. Chem.*, 1970, **42**, 526–529.
52 G. Liu, Y.-J. Fan and J.-L. Zhang, *J. Porphyrins Phthalocyanines*, DOI: 10.1142/S1088424619501608.
53 E. M. Nichols, J. S. Derrick, S. K. Nistanaki, P. T. Smith and C. J. Chang, *Chem. Sci.*, 2018, **9**, 2952–2960.
54 P. Sen, B. Mondal, D. Saha, A. Rana and A. Dey, *Dalton Trans.*, 2019, **48**, 5965–5977.
55 C. Costentin, M. Robert, J.-M. Savéant and A. Tatin, *Proc. Natl. Acad. Sci. U. S. A.*, 2015, **112**, 6882–6886.
56 H. Rao, L. C. Schmidt, J. Bonin and M. Robert, *Nature*, 2017, **548**, 74–77.
57 H. Rao, J. Bonin and M. Robert, *J. Phys. Chem. C*, 2018, **122**, 13834–13839.
58 H. Rao, C.-H. Lim, J. Bonin, G. M. Miyake and M. Robert, *J. Am. Chem. Soc.*, 2018, **140**, 17830–17834.
59 E. A. Mohamed, Z. N. Zahran and Y. Naruta, *Chem. Commun.*, 2015, **51**, 16900–16903.
60 Z. N. Zahran, E. A. Mohamed and Y. Naruta, *Sci. Rep.*, 2016, **6**, 24533.
61 D. Behar, T. Dhanasekaran, P. Neta, C. M. Hosten, D. Ejeh, P. Hambright and E. Fujita, *J. Phys. Chem. A*, 1998, **102**, 2870–2877.
62 O. Enoki, T. Imaoka and K. Yamamoto, *Macromol. Symp.*, 2003, **204**, 151–158.
63 J. D. B. Koenig, J. Willkomm, R. Roesler, W. E. Piers and G. C. Welch, *ACS Appl. Energy Mater.*, 2019, **2**, 4022–4026.
64 B. Mondal, P. Sen, A. Rana, D. Saha, P. Das and A. Dey, *ACS Catal.*, 2019, **9**, 3895–3899.
65 C. M. Lieber and N. S. Lewis, *J. Am. Chem. Soc.*, 1984, **106**, 5033–5034.
66 N. Sonoyama, M. Kirii and T. Sakata, *Electrochem. Commun.*, 1999, **1**, 213–216.
67 Z. Weng, J. Jiang, Y. Wu, Z. Wu, X. Guo, K. L. Materna, W. Liu, V. S. Batista, G. W. Brudvig and H. Wang, *J. Am. Chem. Soc.*, 2016, **138**, 8076–8079.
68 Y. Wu, J. Jiang, Z. Weng, M. Wang, D. L. J. Broere, Y. Zhong, G. W. Brudvig, Z. Feng and H. Wang, *ACS Cent. Sci.*, 2017, **3**, 847–852.
69 S. Aoi, K. Mase, K. Ohkubo and S. Fukuzumi, *Chem. Commun.*, 2015, **51**, 10226–10228.
70 X.-M. Hu, M. H. Rønne, S. U. Pedersen, T. Skrydstrup and K. Daasbjerg, *Angew. Chem., Int. Ed.*, 2017, **56**, 6468–6472.
71 P. T. Smith, B. P. Benke, Z. Cao, Y. Kim, E. M. Nichols, K. Kim and C. J. Chang, *Angew. Chem., Int. Ed.*, 2018, **57**, 9684–9688.
72 C.-H. Lim, A. M. Holder and C. B. Musgrave, *J. Am. Chem. Soc.*, 2013, **135**, 142–154.
73 T. V. Magdesieva, T. Yamamoto, D. A. Tryk and A. Fujishima, *J. Electrochem. Soc.*, 2002, **149**, D89–D95.
74 H. Z. Zhao, Y. Y. Chang and C. Liu, *J. Solid State Electrochem.*, 2013, **17**, 1657–1664.
75 A. Tatin, C. Comminges, B. Kokoh, C. Costentin, M. Robert and J.-M. Savéant, *Proc. Natl. Acad. Sci. U. S. A.*, 2016, **113**, 5526–5529.

76 T. Atoguchi, A. Aramata, A. Kazusaka and M. Enyo, *J. Chem. Soc., Chem. Commun.*, 1991, 156–157.
77 J. Shen, R. Kortlever, R. Kas, Y. Y. Birdja, O. Diaz-Morales, Y. Kwon, I. Ledezma-Yanez, K. J. P. Schouten, G. Mul and M. T. M. Koper, *Nat. Commun.*, 2015, **6**, 8177.
78 D. Quezada, J. Honores, M. García, F. Armijo and M. Isaacs, *New J. Chem.*, 2014, **38**, 3606–3612.
79 D. Quezada, J. Honores, M. J. Aguirre and M. Isaacs, *J. Coord. Chem.*, 2014, **67**, 4090–4100.
80 A. Maurin and M. Robert, *Chem. Commun.*, 2016, **52**, 12084–12087.
81 M. Zhu, J. Chen, L. Huang, R. Ye, J. Xu and Y.-F. Han, *Angew. Chem., Int. Ed.*, 2019, **58**, 6595–6599.
82 A. Maurin and M. Robert, *J. Am. Chem. Soc.*, 2016, **138**, 2492–2495.
83 S. A. Yao, R. E. Ruther, L. Zhang, R. A. Franking, R. J. Hamers and J. F. Berry, *J. Am. Chem. Soc.*, 2012, **134**, 15632–15635.
84 E. A. Mohamed, Z. N. Zahran and Y. Naruta, *Chem. Mater.*, 2017, **29**, 7140–7150.
85 B. Kumar, M. Llorente, J. Froehlich, T. Dang, A. Sathrum and C. P. Kubiak, *Annu. Rev. Phys. Chem.*, 2012, **63**, 541–569.
86 A. J. Sathrum and C. P. Kubiak, *J. Phys. Chem. Lett.*, 2011, **2**, 2372–2379.
87 I. Hod, M. D. Sampson, P. Deria, C. P. Kubiak, O. K. Farha and J. T. Hupp, *ACS Catal.*, 2015, **5**, 6302–6309.
88 N. Kornienko, Y. Zhao, C. S. Kley, C. Zhu, D. Kim, S. Lin, C. J. Chang, O. M. Yaghi and P. Yang, *J. Am. Chem. Soc.*, 2015, **137**, 14129–14135.
89 S. Lin, C. S. Diercks, Y.-B. Zhang, N. Kornienko, E. M. Nichols, Y. Zhao, A. R. Paris, D. Kim, P. Yang, O. M. Yaghi and C. J. Chang, *Science*, 2015, **349**, 1208.
90 C. S. Diercks, S. Lin, N. Kornienko, E. A. Kapustin, E. M. Nichols, C. Zhu, Y. Zhao, C. J. Chang and O. M. Yaghi, *J. Am. Chem. Soc.*, 2018, **140**, 1116–1122.
91 A. R. Battersby, C. J. R. Fookes, G. W. J. Matcham and E. McDonald, *Nature*, 1980, **285**, 17–21.
92 S. Ren, D. Joulié, D. Salvatore, K. Torbensen, M. Wang, M. Robert and C. P. Berlinguette, *Science*, 2019, **365**, 367–369.
93 E. Boutin, M. Wang, J. C. Lin, M. Mesnage, D. Mendoza, B. Lassalle-Kaiser, C. Hahn, T. F. Jaramillo and M. Robert, *Angew. Chem., Int. Ed.*, 2019, **58**, 16172–16176.
94 Y. Wu, Z. Jiang, X. Lu, Y. Liang and H. Wang, *Nature*, 2019, **575**, 639–642.

